Measuring laser carrier-envelope-phase effects in the noble gases with an atomic hydrogen calibration standard

Measuring laser carrier-envelope-phase effects in the noble gases with an atomic hydrogen calibration standard

Champak Khurmi,[1,2] W. C. Wallace,[1,2] Satya Sainadh U,[1,2] I. A. Ivanov,[3,4] A. S. Kheifets,[3]
X. M. Tong,[5,6] I. V. Litvinyuk,[1,2] R. T. Sang,[1,2] and D. Kielpinski[1,2]

[1]*Australian Attosecond Science Facility, Griffith University, Nathan, Queensland, Australia*

[2]*Centre for Quantum Dynamics, Griffith University, Nathan, Queensland, Australia*

[3]*Research School of Physics and Engineering, Australian National University, Canberra, Australian Capital Territory 0200, Australia*

[4]*Center for Relativistic Laser Science, Institute for Basic Science, Gwangju 500-712, Republic of Korea*

[5]*Center for Computational Sciences, University of Tsukuba, Ibaraki, Japan*

[6]*Faculty of Pure and Applied Sciences, University of Tsukuba, Ibaraki, Japan*

We present accurate measurements of carrier-envelope-phase effects on ionization of the noble gases with few-cycle laser pulses. The experimental apparatus is calibrated by using atomic hydrogen data to remove any systematic offsets and thereby obtain accurate CEP data on other generally used noble gases such as Ar, Kr, and Xe. Experimental results for H are well supported by exact time-dependent Schrödinger equation theoretical simulations; however, significant differences are observed in the case of the noble gases.

Frontiers for few-cycle laser pulses are expanding every day with the generation of short extreme-ultraviolet laser pulses from solid-state targets [1] and production of few-cycle laser pulses in the midinfrared domain [2]. Along with innovative ways to generate carrier-envelope-phase (CEP) stable few-cycle laser pulses with multimegahertz repetition rate [3], new techniques are continually explored to accurately measure the laser CEP [4–7].

$$\vec{E}(t) = |\vec{E}(t)| \cos(\omega_0 t + \phi_{CEP}). \quad (1)$$

The electric field of a laser pulse can be described as shown in Eq. (1), where $|\vec{E}(t)|$ is the pulse envelope, ω_0 is the carrier frequency, and ϕ_{CEP} is the CEP of the laser pulse. The CEP specifies the offset between the peak of the pulse envelope and the nearest maximum of the electric field oscillation. An important aspect of the few-cycle laser pulse ($\lambda_{central} = 780$ nm, one optical cycle $\sim$2.6 fs) is that the CEP also affects the processes initiated by the laser pulse when interacting with the matter. The ability to precisely measure the CEP of few-cycle laser pulses is very important for diverse scientific applications such as high-harmonics generation [8,9], above-threshold ionization (ATI) [10], attosecond pulse generation [11–13], coherent control of molecular dynamics [14–17], and attosecond ionization under the influence of strong laser fields [18,19].

Generally, photoionization at different laser peak intensities can be described in two broad domains, (i) the multiphoton ionization domain, where simultaneous absorption of multiple photons results in ejection of an electron from the atomic core causing ionization, and (ii) the photoionization tunneling regime, where the potential barrier of the atom is lowered by the intense laser electric field and the electron tunnels through the Coulomb potential barrier. The emitted electron in the latter case can escape the atomic core potential and hit the detector or it may recombine with the parent ion to give rise to high-harmonics generation [20,21]. The physics behind these processes seems simple but accurately predicting the atomic Coulomb potential and its effects on

the electron wave packet is a major challenge for even the most advanced theoretical methods. Recent efforts by Torlina *et al.* [22] to measure the electron tunneling time also imply the breakdown of key theoretical assumptions in interpreting attoclock measurements for multielectron atoms that are mainly attributed to the delays associated with multielectron dynamics. The work presented in this paper provides accurate and extremely reliable experimental evidence to further the debate in this regard and raise questions regarding the validity of advanced theoretical methods to measure the laser CEP using multielectron atomic species such as Ar, Kr, and Xe.

Experiments by Paulus and co-workers [23] have shown that the CEP of few-cycle laser pulses can be tagged by using Xe atoms as target species. But questions remain about systematic CEP phase offsets in such measurements, since the accuracy of the available theoretical models is not well characterized [24]. However, in the case of atomic hydrogen exposed to an intense few-cycle laser pulse, the time-dependent Schrödinger equation (TDSE) can be solved numerically with high precision and provides a very reliable calibration standard [25–28]. Here, we present the experimental evidence for the measurement of CEP of few-cycle laser pulses in the noble gases by using atomic hydrogen as the calibration standard. In the case of H, we find that the experimental results are well supported by *ab initio* theoretical simulations; however, for multielectron species such as Ar, Kr, and Xe, the single-active electron (SAE) approximation [29] differs significantly from experimental results.

Figure 1 shows a schematic of the experiment. A commercial Femtosecond Compact Pro laser system with CEP stability is used to generate $\sim$6-fs laser pulses with 780-nm central wavelength at 1-kHz repetition rate. An additional f-$2f$ interferometer (from Menlo Systems) is used to establish CEP feedback and locking near the experimental end station to control slow CEP drifts. A set of matched fused silica wedges (from MolTech GmbH Berlin, 1-mm lateral translation = 1.25 rad rad phase shift) is used to vary the CEP of the laser pulses.
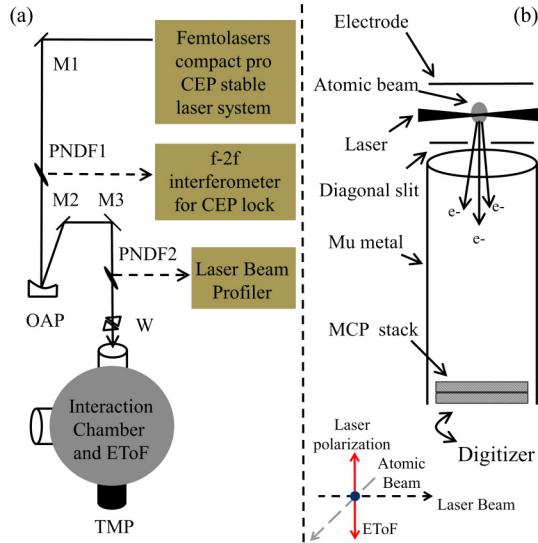
FIG. 1. (a) Experimental setup for CEP resolved experiments. M1–M3: Reflective mirrors; PNDF: pellicle neutral density filters; OAP: off-axis parabolic mirror; W: fused silica wedge; TMP: turbomolecular pump. (b) Electron-time-of-flight spectrometer. Atomic beam (gray, long dash), laser beam (black, short dash), and laser polarization (red, solid line) directions are shown on bottom left of (b) in a laboratory frame.

The experimental setup to create an atomic H beam has been described in detail elsewhere [30]. The atomic H beam is accompanied by residual H_2 and background contributions in the interaction chamber (see the Supplemental Material for more details [31]). At each intensity, three separate laser CEP resolved measurements are taken to isolate atomic H photoelectron yield, namely, with the atomic H source ON ($H + H_2$ + background), atomic H source OFF (H_2 + background), and only background. In the case of noble gases, two separate laser CEP resolved measurements are taken, with noble gas source ON (noble gas+background) and background only. All these measurements are performed at the same phase points by repeating the wedge scan with f-$2f$ phase lock; therefore all systematic errors because of H_2 and background contributions are canceled out. The systematic errors resulting from change of dissociation fraction ($\pm 5\%$) of H_2 to atomic H contribute ~2% error to the final atomic H photoelectron yield (see the Supplemental Material for more details [31]).

The laser beam is focused into the interaction chamber by using an off-axis parabolic (OAP, focal length = 750 mm, spot size = 45 μm, Rayleigh length ~10 cm) mirror; it interacts with the atomic H beam in the interaction chamber (polarization = perpendicular to gas flow and along the time-of-flight axis of the spectrometer, atomic beam diameter ~0.5 mm). The peak intensity of the laser pulses was estimated by measuring focal spot size, pulse width, and average laser energy. Electrons generated from this interaction are detected by an electron-time-of-flight detection system (EToF). Electrons emitted in only one direction are collected. The EToF spectrometer [Fig. 1(b)] is enclosed in μ-metal to provide shielding from stray magnetic fields. Electrons with different kinetic energies are generated from laser and atom interaction
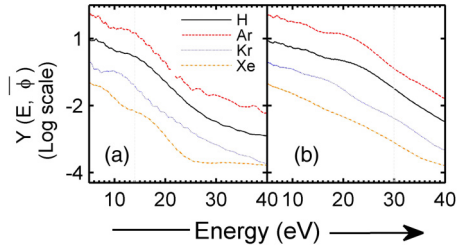

FIG. 2. CEP averaged electron energy spectra of different atomic species, namely, Ar (red, dash), H (black, solid), Kr (blue, dotted), and Xe (orange, dot-dash) at two different intensities. (a) $1.2 \times 10^{14} W/cm^2 (U_p = 7\,eV)$ and (b) $2.5 \times 10^{14} W/cm^2 (U_p = 15\,eV)$. Electron energy spectra for different atomic species are offset for the sake of clarity. Solid vertical lines represent $2U_p$ point. The y axis has arbitrary units with a $\log_{10}$ scale.

and travel in a field-free region to a microchannel plate. Each electron gives rise to a temporally resolved voltage peak which is recorded using an analog-to-digital conversion card (Agilent, model no. U1084A). Figure 2 shows the CEP averaged electron energy spectra of different atomic species at two laser peak intensities, namely, at 1.2×10^{14} and $2.5 \times 10^{14} W/cm^2$ (ponderomotive energy $U_p = 7$ and 15 eV, respectively). Solid vertical lines in Fig. 2 represent the $2U_p$ point which marks the onset of the rescattering domain, where the emitted electron gains enough quiver energy from the laser field to either rescatter from the parent ion or cause further ionization. The electron energy spectra for each atomic species have been offset for the sake of clarity. For CEP resolved experiments, a motorized fused silica wedge is used to vary the laser CEP over a range exceeding 2π rad.

The electron energy spectrum is collected at each wedge position (integration time 90 s) representing a laser CEP point. The CEP-dependent electron spectrum is denoted $Y(E,\varphi)$, where E is the electron kinetic energy and ϕ is the laser CEP. As seen from Fig. 2, $Y(E,\bar{\phi})$, which is the laser CEP averaged electron energy spectrum, varies over a wide range so we parametrize the laser CEP effects by the normalized quantity $S(E,\varphi)$ that measures the CEP effect at E relative to the CEP averaged electron yield at E.

$$S(E,\phi) = \frac{Y(E,\phi) - Y(E,\bar{\phi})}{Y(E,\bar{\phi})}. \qquad (2)$$

We obtain theoretical simulations for H from numerical integration of the three-dimensional TDSE. These simulations are extremely reliable as demonstrated by our previous work [28]. For multielectron systems such as Ar, Kr, and Xe, the theoretical simulations are based on SAE approximation. The ATI spectra of the rare gas atoms are calculated by solving the TDSE with the generalized spectrum in the energy representation [29,32] under the single-active electron approximation. We use the model potentials [33] obtained by density functional theory with the self-interaction correction [34], which gives the atomic ionization potentials. Focal volume averaging is performed on all simulations for comparison with experimental data.

Figures 3 and 4 show the CEP calibrated experimental data and theoretical simulations for H, Ar, Kr, and Xe. For ease of viewing, both data and theory are smoothed with respect
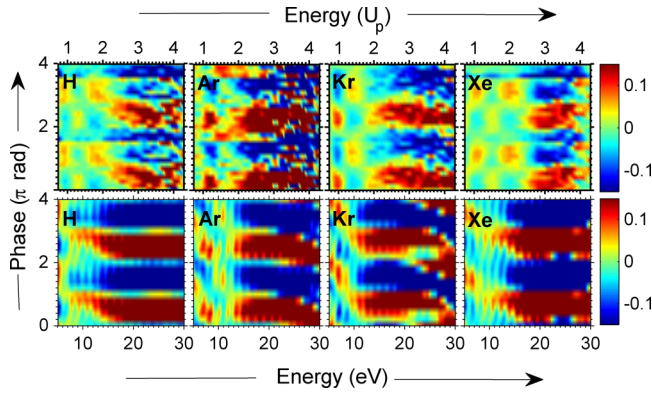
FIG. 3. CEP maps based on Eq. (1) for different atomic species at 1.2×10^{14} W/cm^2 ($U_p = 7$ eV). Top panel (left to right): CEP calibrated experimental results for H, Ar, Kr, and Xe. Bottom panel (left to right): theory data. In the case of H exact TDSE simulations are used, whereas for Ar, Kr, and Xe, theoretical simulations are based on SAE approximations. The bottom x axes are in units of photoelectron energy and the top x axes are in units of U_p.

to energy using a Gaussian filter with a full width at half maximum (FWHM) of 1.5 eV and the results over the CEP range $0 < \varphi < 2\pi$ are replicated over the range $2\pi < \varphi < 4\pi$. The Gaussian filter with 1.5 eV FWHM was chosen based on the energy resolution of the EToF detector. Depending upon the ponderomotive energy (U_p) of the photoelectron, the results shown in Figs. 3 and 4 can be separated into two domains, namely, above and below $2U_p$, as the photoelectrons in these domains come from two different mechanisms. Below $2U_p$, the photoelectron can come from the tunneling mechanisms caused by one of the several laser electric field peaks (i.e., tunneling occurs over a varied range of phases of the fundamental pulse) and from the subsequent rescattering process from the parent ion. The laser CEP dependence in this regime also depends on the energy of the photoelectron and
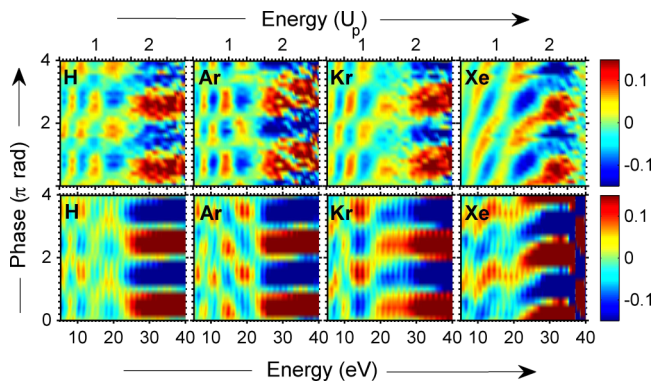

FIG. 4. CEP maps based on Eq. (1) for different atomic species at 2.5×10^{14} W/cm^2 ($U_p = 15$ eV). Top panel (left to right): CEP calibrated experimental results for H, Ar, Kr, and Xe. Bottom panel (left to right): Theoretical simulations; in the case of H exact TDSE simulations are used, whereas for Ar, Kr, and Xe, theoretical simulations are based on SAE approximations. The bottom x axes are in units of photoelectron energy and the top x axes are in units of U_p.
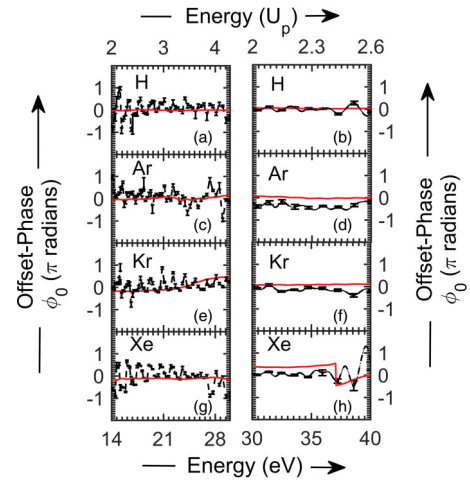

FIG. 5. This figure shows a qualitative comparison of experimental and theoretical data for $\geqslant 2U_p$ photoelectron energy spectrum for both intensity regimes. The experimental data are shown with a dotted line (black) and theoretical data are represented by a solid line (red). The left-hand side column [namely, (a) H, (c) Ar, (e) Kr, and (g) Xe] represents the 1.2×10^{14} W/cm^2 intensity regime and the right-hand side column [namely, (b) H, (d) Ar, (f) Kr, and (h) Xe] represents 2.5×10^{14} W/cm^2 intensity regime, respectively. In the case of H (a,b), experimental data are compared with exact TDSE simulations, whereas in the case of noble gases (c–h), SAE approximations are used for theoretical simulations. The bottom x axes are in units of photoelectron energy and the top x axes are in units of U_p.

therefore makes the calibration of laser CEP more complicated [35]. However, the photoelectrons above $2U_p$ originate from a different mechanism. Above $2U_p$, the photoelectrons come from back rescattering from the parent ion. The energy of the photoelectron depends on the largest peak in the laser electric field and the yield of these photoelectrons depends on the peak field strength before the largest one [29]. In this domain, the dependence of laser CEP on the energy and yield of the photoelectron is more stable and we use this domain to calibrate the laser CEP.

It is evident from Figs. 3 and 4 that in the case of H for $\geqslant 2U_p$, we observe good agreement between experimental data (top panel) and TDSE simulations (bottom panel). It demonstrates that the experimental results are reliable. The experimental data for the noble gases are taken under identical conditions in the same apparatus, so they are expected to be similarly reliable. We can therefore assign an absolute CEP to the data on the noble gases free of systematic errors.

For further qualitative analysis, a line-out comparison [Figs. 5(a)–5(h)] is shown between experimental (dotted line, black) data and theoretical simulations (solid line, red) for photoelectron energy of $\geqslant 2U_p$ for both intensity regimes (see the Supplemental Material for full comparison [31]). For the higher-intensity regime (Fig. 5, right column), in the case of H [Fig. 5(b)], the experimental data and TDSE simulations show good overlap, but the qualitative trends for Ar, Kr, and Xe [Figs. 5(d), 5(f), and 5(h)] show $>0.25\pi$ rad phase offset between experiment and SAE simulations. For the lower-intensity regime (Fig. 5, left column), in the case of H [Fig. 5(a)], there is good agreement between experiment
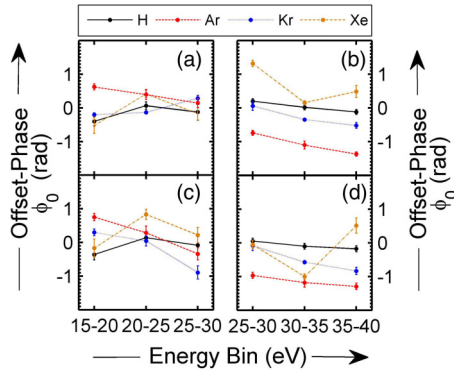
FIG. 6. Experimental phase offset (bin width = 5 eV) for different atomic species at (a) 1.2×10^{14} W/cm^2 and (b) 2.5×10^{14} W/cm^2. Difference between phase offset from experiment and theoretical simulations for (c) 1.2×10^{14} W/cm^2 and (d) 2.5×10^{14} W/cm^2. Lines are a guide to the eye. Note that the *y* axes in this figure are in units of radians.

and TDSE simulations at $\geqslant 3U_p$ but between $2U_p$ and $3U_p$, the data show a higher signal-to-noise ratio. Similarly, in the case of noble gases [Figs. 5(c), 5(e), and 5(g)], although there is significant qualitative overlap between theory and experiment, the experimental data show a higher signal-to noise-ratio.

For quantitative analysis of the CEP effects, we bin the data and simulations with respect to energy. A bin width of 5 eV was found to represent a good compromise between the signal-to-noise ratio and energy resolution. We fit these data to a sinusoidal function for the CEP effects, as shown in Eq. (3).

$$B_E(\phi) = A \sin(\phi + \phi_0) \qquad (3)$$

where the data in the bin centered on energy E are denoted $B_E(\varphi)$ [Eq. (3)], and φ_0 is the "offset" phase and A is the amplitude. This offset phase obtained from experimental data is plotted for each atomic species in Figs. 6(a) and 6(b) for 1.2×10^{14} and 2.5×10^{14} W/cm^2, respectively. The difference between the estimated experimental and theoretical offset phases is shown in Figs. 6(c) and 6(d) for both laser intensities, respectively (note that the *y* axes in these figures

are in units of radians). It is evident that the experimental offset phase for H is in good agreement with the theoretical predictions in both intensity regimes. For the noble gases, the quantitative analysis shows two principal points of difference between experiment and theory; first, in the energy region above $2U_p$, contrary to the SAE simulations, the observed CEP effects depend on the photoelectron energy; second, the SAE simulations display a large systematic offset in CEP relative to the actual values obtained from the TDSE simulations. It is important to note that only the use of experimental evidence from H calibration can reveal this offset, since SAE (for multielectron atoms) and direct TDSE (for H) can never be directly compared by purely theoretical means.

An accurate interpretation of the physical phenomenon responsible for these complex CEP resolved photoelectron energy spectra is not trivial. Any such attempts to assign a particular mechanism responsible for observed spectra would heavily depend on the key theoretical assumptions in estimating atomic Coulomb potential, electron rearrangement dynamics after light absorption, and the effect of long-range Coulomb potential on the electron wave packet before it hits the detector. Recent experiments [36] on He atoms using few-cycle laser pulses also suggest that at higher intensities (2–4×10^{14} W/cm^2) the electron correlation effects of bound-state electrons play a significant role in determining the time resolved absorption spectra of autoionizing states. In this paper, the extremely reliable and accurate measurements of the phase offset in H-referenced noble gases are used to expose the weakness of theoretical models based on SAE approximations. These experimental results clearly demonstrate that it is not possible to rely on approximate theoretical methods such as SAE to accurately calibrate the CEP of the few-cycle laser pulses using noble gases. The results from this work can be used to guide and validate all future multielectron theoretical simulations to accurately measure the laser CEP.

[1] T. T. Luu, M. Garg, S. Y. Kruchinin, A. Moulet, M. T. Hassan, and E. Goulielmakis, Nature **521**, 498 (2015).

[2] D. Novoa, M. Cassataro, J. C. Travers, and P. S. J. Russell, Phys. Rev. Lett. **115**, 033901 (2015).

[3] O. Pronin *et al.*, Nat. Commun. **6**, 6988 (2015).

[4] T. Paasch-Colberg *et al.*, Nat. Photonics **8**, 214 (2014).

[5] T. M. Fortier, P. A. Roos, D. J. Jones, S. T. Cundiff, R. D. R. Bhat, and J. E. Sipe, Phys. Rev. Lett. **92**, 147403 (2004).

[6] M. Mehendale, S. A. Mitchell, J. P. Likforman, D. M. Villeneuve, and P. B. Corkum, Opt. Lett. **25**, 1672 (2000).

[7] M. Kresz *et al.*, Nat. Phys. **2**, 327 (2006).

[8] I. P. Christov, M. M. Murnane, and H. C. Kapteyn, Phys. Rev. Lett. **78**, 1251 (1997).

[9] C. A. Haworth, L. E. Chipperfield, J. S. Robinson, P. L. Knight, J. P. Marangos, and J. W. G. Tisch, Nat. Phys. **3**, 52 (2007).

[10] F. Grasbon, G. G. Paulus, H. Walther, P. Villoresi, G. Sansone, S. Stagira, M. Nisoli, and S. De Silvestri, Phys. Rev. Lett. **91**, 173003 (2003).

[11] A. Baltuska *et al.*, Nature **421**, 611 (2003).

[12] G. Sansone *et al.*, Science **314**, 443 (2006).

[13] R. Kienberger *et al.*, Science **297**, 1144 (2002).

[14] V. R. Bhardwaj, S. A. Aseyev, M. Mehendale, G. L. Yudin, D. M. Villeneuve, D. M. Rayner, M. Y. Ivanov, and P. B. Corkum, Phys. Rev. Lett. **86**, 3522 (2001).

[15] X. M. Tong and C. D. Lin, Phys. Rev. Lett. **98**, 123002 (2007).

[16] J. Itatani, J. Levesque, D. Zeidler, H. Niikura, H. Pepin, J. C. Kieffer, P. B. Corkum, and D. M. Villeneuve, Nature **432**, 867 (2004).

[17] H. Li, B. Mignolet, G. Wachter, S. Skruszewicz, S. Zherebtsov, F. Süßmann, A. Kessel, S. A. Trushin, N. G. Kling, M.

Kübel, B. Ahn, D. Kim, I. Ben-Itzhak, C. L. Cocke, T. Fennel, J. Tiggesbäumker, K.-H. Meiwes-Broer, C. Lemell, J. Burgdörfer, R. D. Levine *et al.*, Phys. Rev. Lett. **114**, 123004 (2015).

[18] P. Eckle, A. N. Pfeiffer, C. Cirelli, A. Staudte, R. Doerner, H. G. Muller, M. Buettiker, and U. Keller, Science **322**, 1525 (2008).

[19] O. Pedatzur *et al.*, Nat. Phys. **11**, 815 (2015).

[20] A. de Bohan, P. Antoine, D. B. Milošević, and B. Piraux, Phys. Rev. Lett. **81**, 1837 (1998).

[21] M. Nisoli, G. Sansone, S. Stagira, S. De Silvestri, C. Vozzi, M. Pascolini, L. Poletto, P. Villoresi, and G. Tondello, Phys. Rev. Lett. **91**, 213905 (2003).

[22] L. Torlina *et al.*, Nat. Phys. **11**, 503 (2015).

[23] G. G. Paulus, F. Lindner, H. Walther, A. Baltuska, E. Goulielmakis, M. Lezius, and F. Krausz, Phys. Rev. Lett. **91**, 253004 (2003).

[24] G. G. Paulus, Laser Phys. **15**, 843 (2005).

[25] W. C. Wallace *et al.*, New J. Phys. **15**, 033002 (2013).

[26] M. G. Pullen, W. C. Wallace, D. E. Laban, A. J. Palmer, G. F. Hanne, A. N. Grum-Grzhimailo, K. Bartschat, I. Ivanov, A. Kheifets, D. Wells, H. M. Quiney, X. M. Tong, I. V. Litvinyuk, R. T. Sang, and D. Kielpinski, Phys. Rev. A **87**, 053411 (2013).

[27] A. M. Sayler *et al.*, Opt. Lett. **40**, 3137 (2015).

[28] W. C. Wallace, O. Ghafur, C. Khurmi, S. Sainadh U, J. E. Calvert, D. E. Laban, M. G. Pullen, K. Bartschat, A. N. Grum-Grzhimailo, D. Wells, H. M. Quiney, X. M. Tong, I. V. Litvinyuk, R. T. Sang, and D. Kielpinski, Phys. Rev. Lett. **117**, 053001 (2016).

[29] X. M. Tong, K. Hino, and N. Toshima, Phys. Rev. A **74**, 031405 (2006).

[30] M. G. Pullen *et al.*, Opt. Lett. **36**, 3660 (2011).

[31] See Supplemental Material at http://link.aps.org/supplemental/10.1103/PhysRevA.96.013404 for isolation of atomic hydrogen signal, systematic H_2 error estimation and Fig. 5 with full energy scale.

[32] X.-M. Tong and S.-I. Chu, Chem. Phys. **217**, 119 (1997).

[33] X. M. Tong and C. D. Lin, J. Phys B: At., Mol. Opt. Phys. **38**, 2593 (2005).

[34] X.-M. Tong and Shih-I. Chu, Phys. Rev. A **55**, 3406 (1997).

[35] D. B. Milošević and F. Ehlotzky, Phys. Rev. A **58**, 3124 (1998).

[36] C. Ott *et al.*, Nature **516**, 374 (2014).